

The spatial resolution performance of a time-resolved optical imaging system using temporal extrapolation

Jeremy C. Hebden, David J. Hall, and David T. Delpy

Department of Medical Physics, University College London, 11-20 Capper Street, London WC1E 6JA, England

(Received 22 March 1994; accepted for publication 18 October 1994)

Optical imaging methods are being explored as a potential means of screening for breast cancer. Previous investigations of time-resolved imaging techniques have suggested that due to the lack of photons with sufficiently small pathlengths, the spatial resolution achievable through a human breast would be unlikely to be better than a centimeter. Experimental results presented here indicate, however, that higher resolution may be achieved by extrapolating the measured temporal distribution of transmitted photons. This is performed using a least-squares fit between data and an analytic model of photon transport. The spatial resolution of a time-resolved imaging system was evaluated by measuring the edge response produced by an opaque mask embedded in the center of a 51-mm-thick, very highly scattering medium. The limiting spatial resolution was improved from about 13 mm to about 5 mm.

Key words: optical imaging, time-of-flight, spatial resolution, breast imaging

I. INTRODUCTION

In the United States and Europe several tens of thousands of women die each year from breast cancer, many of whom may have survived had their disease been diagnosed at an earlier stage of its development.^{1,2} Although a more widespread use of x-ray mammography could substantially reduce mortality, there is clearly a need for more effective, less expensive, and safer screening methods. The idea that optical radiation might be used as a means of obtaining diagnostic images of the breast has been around at least since Cutler³ first presented breast images in 1929. Studies have demonstrated, however, that the overwhelming scatter of light in tissue severely limits the clinical utility of transillumination imaging methods.⁴ Reported measurements of the optical properties of breast tissues reveal that no light can penetrate more than a few millimeters without being scattered a large number of times.⁵ The advent of picosecond pulse lasers, particularly in the near-infrared wavelength regime, and fast optical detectors able to resolve such pulses, has led to a revival of interest in the problem of optical imaging through tissue.^{6,7} Whereas straightforward intensity measurements are dominated by photon interactions at the surface of a scattering object, information on the internal optical properties of an object can be provided to a much greater degree by using the temporal distribution of transmitted light.

Researchers have examined a wide variety of methods of obtaining temporal information and of generating images. The methods of most relevance to the work described here are those that involve isolating a small amount of transmitted light that is scattered along a path close to a straight line between the source and detector. The magnitude of this small fraction is dependent upon the optical properties of the medium along that line and may be used to construct a transmission image. If the medium is not too highly scattering, coherent detection methods may be utilized. These exploit the fact that a continuous laser beam that undergoes severe scatter is rendered incoherent, and the task is to measure the interference between the least-scattered signal of interest that

retains some coherence and a reference beam.⁸ In the presence of more severe scatter, the discrimination between transmitted photons can be performed by illuminating the object with a short pulse of light and measuring their times-of-flight. The relative intensity of the earliest-arriving photons can be enhanced by using a Kerr shutter⁹ or Raman amplifier,¹⁰ or the temporal profile of the transmitted light can be obtained directly using a streak camera^{11,12} or a fast amplifier-microchannel plate device.¹³ By whatever means the measurements are made, it is generally assumed that an image with the highest possible spatial resolution requires the use of light with the shortest possible flight times. The vast majority of transmitted photons with longer paths within the medium are discarded.

Experiments have shown that, as expected, an increase in spatial resolution correlates with a decrease in minimum flight time,¹⁴ and theoretical models have been developed to predict the spatial resolution performance of time-resolved imaging techniques.^{15,16} However, if the isolation of short pathlength photons is a necessary condition for acquiring adequate spatial resolution for breast imaging, then there is now strong evidence that a scarcity of photons with sufficiently short pathlengths will limit the spatial resolution to no better than about a centimeter.^{17,18} As a consequence, it is desirable to explore whether higher resolution information can be extracted from longer pathlength photons.

While it is true that only the shortest pathlength photons are known to have remained within a narrow volume surrounding the line-of-sight between the source and detector, the presence of a small anomalous absorbing or scattering region centered on the line-of-sight will influence transmitted photons of *all* pathlengths. However, it is not evident to what degree high-resolution image information can be inferred from the distribution of the longer path photons. Recently we have been interested in the possibility that the short-pathlength component of the temporal distribution of transmitted light can be inferred to some degree by extrapolation of the measured distribution to shorter times. We have attempted to estimate the intensity of short pathlength photons

by comparison of experimental data to an analytical model, which is fit to all or part of the available temporal distribution. The fits are used simply as high signal-to-noise ratio (SNR) representations of the original data, and the noiseless predictions of short time-of-flight photon intensities arise exclusively from the model fitted over substantially longer times. This method cannot, of course, generate high-resolution information from data in which it is not already contained. The potential utility of the method depends entirely on how accurately the model can represent the true population of short pathlength photons.

Time-resolved imaging using a streak camera as a detector involves translating the line-of-sight between the source and detector in two dimensions over the surface of the object, and measuring the temporal distribution of transmitted photons at each position. Images are produced from the intensity integrated over a period of time Δt immediately following the instant at which the earliest possible photon (i.e., an unscattered photon) would be detected. Recently, the principle of temporal extrapolation was tested by obtaining images through a highly scattering medium at integration times short enough for the actual number of photons with such short flight-times to be below the measurable limit.¹⁹ The images revealed internal structure of the medium with a contrast and spatial resolution significantly better than that achievable from the experimental data directly. The objective of the work presented here has been to produce a quantitative estimate of the gain in spatial resolution performance obtainable using temporal extrapolation.

II. THEORY

A. Analytical models of photon transport

The published literature provides several analytical models of the temporal behavior of light propagating through homogeneous scattering and absorbing media for various geometrical arrangements. We examined two models for a slab geometry as potential means of extrapolating our experimental data. One model, presented by Patterson *et al.*²⁰ (PCW), is based on the diffusion approximation to the radiative transfer theory. Another, described by Gandjbakhche *et al.*²¹ (GWBN), is based on random walk theory. Both models suffer from the disadvantage that the scatter is assumed to be isotropic, but both have the significant advantage that the mathematics is relatively simple to implement in a least-squares fitting routine. Each model provides an analytic expression, $T(\rho, d, t)$, for the time-dependent distribution of transmitted intensity detected at a distance ρ from the optical axis on the surface of a slab of homogenous scattering material of thickness d and refractive index n when illuminated by a pulse of negligible duration at a point on the opposite surface. The expression for the PCW model is as follows:

$$T(\rho, d, t) = AD^{-3/2}(t-t_0)^{-5/2}e^{-\mu_a c(t-t_0)}e^{-\rho^2/4Dc(t-t_0)}Q(d, t), \tag{1}$$

where $Q(d, t)$ is a source dipole term given by

$$Q(d, t) = \sum_{n=1, k=2n-1}^{n=\infty} \left[(kd-z_0)\exp\left(\frac{-(kd-z_0)^2}{4Dc(t-t_0)}\right) - (kd+z_0)\exp\left(\frac{-(kd+z_0)^2}{4Dc(t-t_0)}\right) \right]. \tag{2}$$

The parameter μ_a is the absorption coefficient and z_0 is the reciprocal of the transport scattering coefficient, μ'_s , defined as $\mu_s(1-g)$, where μ_s is the scatter coefficient and g is the mean cosine of scatter. The parameter D is the diffusion coefficient, defined as $\frac{1}{3}(\mu_a + \mu'_s)^{-1}$. The parameter A represents an arbitrary amplitude and t_0 the position of the function on the time axis. Our implementation of the PCW model is described comprehensively elsewhere.¹⁹ The GWBN model, based upon Eq. (A2) of the paper by Gandjbakhche *et al.*,²¹ is as follows:

$$T(\rho, d, t) = A\sqrt{\mu'_s}(t-t_0)^{-3/2}e^{-\mu_a c(t-t_0)}e^{-3\mu'_s \rho^2/4c(t-t_0)}W(d, t), \tag{3}$$

where $W(d, t)$ is given by

$$W(d, t) = \sum_{k=-\infty}^{k=\infty} \left[\exp\left(\frac{-3[(2k+1)(\mu'_s d + \sqrt{2}) - \sqrt{8}]^2}{4\mu'_s c(t-t_0)}\right) - \exp\left(\frac{-3[(2k+1)(\mu'_s d + \sqrt{2})]^2}{4\mu'_s c(t-t_0)}\right) \right]. \tag{4}$$

Note a factor μ'_s was accidentally omitted from the numerator of each exponential within the infinite series term in Eq. (A2) of Gandjbakhche *et al.*²¹ Implementation of this model followed precisely the same procedure as that for the PCW model. In both cases we integrated $T(\rho, d, t)$ over a finite aperture of radius R centered on the line-of-sight through the slab. Both models are described by four parameters that are permitted to vary during the data fitting process: the absorption coefficient μ_a , the transport scattering coefficient μ'_s , the amplitude A , and temporal offset t_0 . We applied each of these models to the analysis of the data described below and discovered that there was negligible difference in the results. The two curves generated for a fit to any single experimental temporal distribution appeared to be almost indistinguishable, although the optical parameters used to produce identical shapes were not precisely the same. However, because both models are based on isotropic migration their similarity is not surprising.

B. Spatial resolution evaluation

The spatial resolution measurements described here were performed using the method developed by Bentzen.²² The method is based upon the reasonable assumption that the line spread function (LSF) of an imaging system may be approximated by a Gaussian distribution. The LSF for a linear system is the derivative of the edge response function (ERF), and Bentzen provides an approximate expression for the finite integral of a Gaussian, consisting of an inverse polynomial. A previous application of this method to a time-resolved imaging system is described elsewhere.¹⁴ While

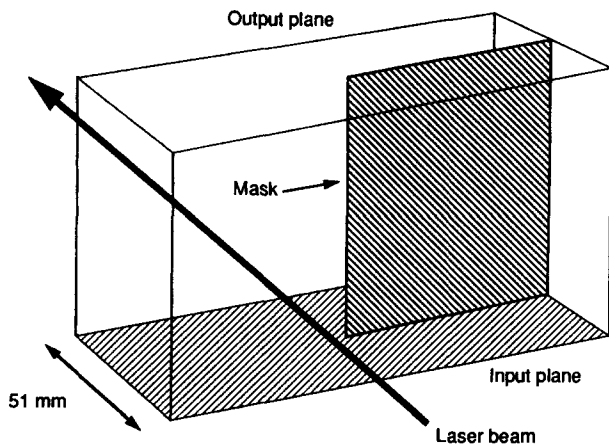


FIG. 1. The object used for measuring the ERF of the imaging system.

results achieved so far appear to be sensible, it should be noted that time-resolved imaging is nonlinear and therefore the Bentzen method should be applied with some caution. The ERF may be obtained, as described below, by recording the modulation in signal corresponding to the detection of a sharp boundary between media of highly contrasting transmittance. The inverse polynomial may be fitted to the measured signal, and thereby four parameters (and their associated uncertainties) are obtained which describe the response: the edge position (m), the maximum (C_1) and minimum (C_2) intensities of the edge profile, and a width parameter (σ) corresponding to the standard deviation of the corresponding Gaussian LSF. Since the MTF of the system is equal to the Fourier modulus of the LSF, the width parameter is inversely proportional to the spatial frequency at which the MTF falls to some arbitrary fraction of its maximum.¹⁴ The spatial resolving power of a medical imaging system is often defined as that corresponding to a 10% response on the MTF curve, which can be shown¹⁴ implies a spatial resolution given by $\Delta x \approx 2.93\sigma$.

III. EXPERIMENTAL METHOD

Time-resolved measurements of the distribution of light transmitted through highly scattering media are obtained with a picosecond optical system described elsewhere.¹⁹ Its principal components are a laser source of near-infrared pulses and a streak camera. In order to obtain ERFs from which the spatial resolution could be evaluated, we used an object similar to that employed for an earlier investigation,¹⁴ shown in Fig. 1. A rectangular transparent plastic box, of internal dimensions $150 \times 100 \times 51$ mm, contains an opaque mask, located parallel to, and halfway between, the two largest sides. The vertical edge of the mask is located roughly halfway between the two smallest sides. The box contained a scattering solution consisting of an aqueous suspension of $1.27\text{-}\mu\text{m}$ -diam latex microspheres, corresponding to values of $g=0.918$ and $\mu_s=9.80\text{ mm}^{-1}$ at 790 nm , the wavelength at which the experiments were performed. This corresponds

to a transport scattering coefficient μ'_s of 0.803 mm^{-1} . A near-infrared dye was also added that produced an absorption coefficient of $\mu_a=0.010\text{ mm}^{-1}$. These coefficients are not far below the mean values expected for a human breast.⁵

The object was illuminated with a beam of pulses with a mean power of 1.4 W over an area about 2 mm in diameter. Transmitted light emerging from the surface directly opposite was relayed to the input slit of the streak camera via a 3-mm -wide optical fiber bundle. The streak images were averaged along the spatial direction to produce intensity versus time profiles with a temporal resolution in the range between 10 and 30 ps , depending on the selected streak speed. A reference pulse was also provided directly from the laser to the streak camera in order to enable the absolute time delay produced by the object to be determined. The object was translated horizontally a distance of 50 mm in 1-mm steps as the temporal distribution was recorded at each position. The streak camera integrated the transmitted light for between 5 and 50 s , with the integration time increasing as the mask moved across the optical axis. The vertical edge of the mask intercepted the optical axis precisely midway through the 50-mm translation. The resulting data consisted of 51 intensity versus time profiles, digitized at intervals of about 4.5 ps . Most ($>90\%$) of the distribution could be sampled within the available window (512 intervals, or 2.3 ns). Compensations were made for various sources of noise and nonlinearities in the system. This includes subtraction of the dark current produced by the CCD camera, adjustment of the streak image intensities to account for the variation in gain across the face of the streak camera detector, and correction for the nonlinearity of the streak camera's sweep rate along the temporal axis. The linearity correction is performed by rescaling data profiles using a set of pre-calculated coefficients. At an early stage of the data processing the center of each reference pulse is identified, and the horizontal axis of each profile is adjusted so that the time at which the earliest transmitted (i.e., unscattered) photon could be detected corresponds to zero. The error involved in the identification of pulse centers, and in the linearity correction process, are sources of possible noise in the final data, as discussed later.

The 51 corrected profiles represent the true temporal distribution of the transmitted light convolved with the response of the detector. The latter can be considered to be a smooth, narrow function with a full-width half-maximum of about 20 ps , plus a very broad, low power component (a few percent of the narrow component) due to the scatter of light in the optics that couple the CCD camera to the rear of the streak camera. Removal of, or at least compensation for, this broad component represents a significant difficulty in time resolving imaging using a streak camera. The effect of this broad component is to cause the temporal distribution of light to appear located upon a broad, low-power Gaussian-like background. We attempt to remove most of this background as follows. First, a Gaussian function is least-squares fitted to the observed intensity at negative times (where only the background exists), while forcing the center of that Gaussian to occur at the position corresponding to the approximate center of gravity of the temporal distribution. Second, the fitted Gaussian is subtracted from the entire distribution.

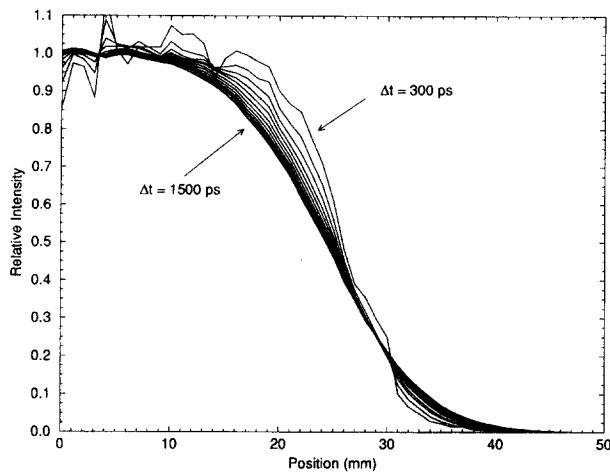


FIG. 2. ERFs obtained from the time-resolved transmittance data for integration times between 300 and 1500 ps, at intervals of 100 ps.

Considering its influence not to be significant, we make no attempt to compensate for the very small additional broadening of the distribution due to convolution with the narrow component of the system response. Finally, in order to investigate the potential utility of temporal extrapolation to enhance imaging performance, two sets of ERFs were generated. First, directly from the 51 temporal profiles, and then from 51 model profiles obtained from least-squares fits to the data.

IV. RESULTS

A. Spatial resolution derived from data profiles

ERFs were obtained by integrating the intensity of each temporal distribution between zero and a specified integration time Δt , and then displaying the integrated intensities as a function of the displacement across the edge of the mask. Figure 2 shows a series of normalized ERFs obtained from the data profiles for $\Delta t = 300$ to 1500 ps at intervals of 100 ps. The vertical axis represents the relative intensity of detected light, and the horizontal axis represents the position of the optical axis relative to the object, in millimeters. The actual location of the edge of the mask is 25 ± 1 mm. As observed in earlier experiments,¹⁴ the signal-to-noise ratio (SNR) decreases with decreasing Δt , and there is a gradual increase in the slope of the curves as Δt decreases, indicating an increase in spatial resolution. As the integration time is decreased below 300 ps, the SNR becomes very low. Figure 3 shows the ERF obtained for $\Delta t = 100$ ps. The manifestation of an "edge" (i.e., a gradient in the integrated intensity) is due almost entirely to the fact that residual background intensity remaining after the subtraction of a Gaussian fit to the scatter component is greater for data acquired on the side of the edge where the optical axis is unobscured by the mask.

The Bentzen ERF model, as described above, was fitted using a least-squares algorithm to each of the data ERFs. Each fit produced an estimate of the width parameter σ , and therefore of the spatial resolution Δx . The values of Δx and

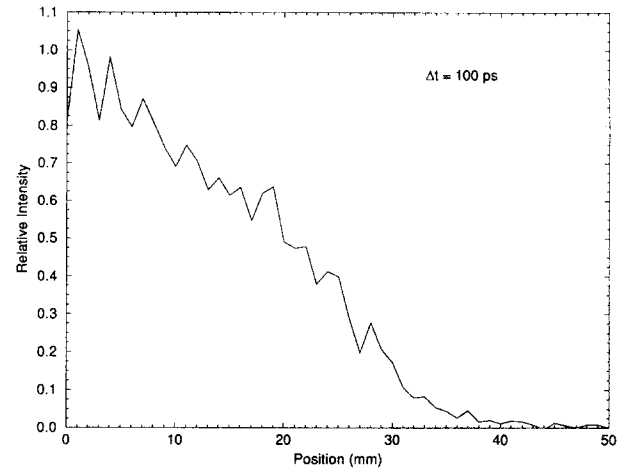


FIG. 3. The ERF obtained from the time-resolved transmittance data for an integration times of 100 ps.

their associated uncertainties derived from the curve fitting process are plotted against Δt in Fig. 4. The figure confirms that there is a steady improvement in spatial resolution as Δt is decreased. However, due to insufficient signal for Δt less than 300 ps the spatial resolution appears to be limited to about 13 mm.

B. Spatial resolution derived from a photon transport model

As mentioned above, both of the analytical models of photon transport that were investigated assume isotropic scatter in a homogeneous medium. Such models can adequately be applied to anisotropic scatter, such as our microsphere solution, by rescaling dimensions by a factor of $(1 - g)$, i.e., by using the transport scatter coefficient μ'_s in place of the scatter coefficient μ_s . The object described here, however, which includes an opaque mask at varying proximity to the optical axis, certainly cannot be said to be homo-

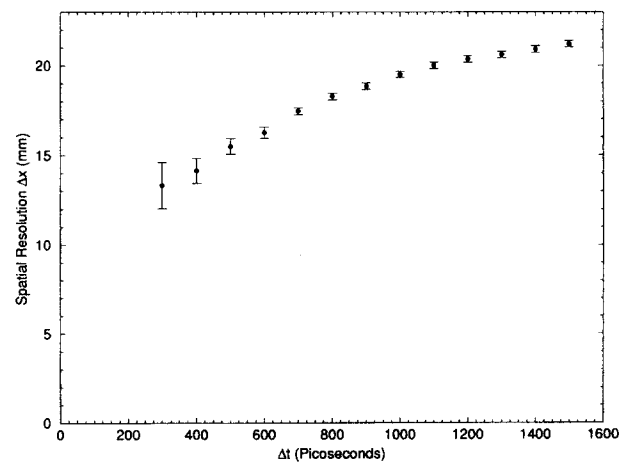


FIG. 4. The estimated spatial resolution as a function of integration time derived directly from the transmittance data.

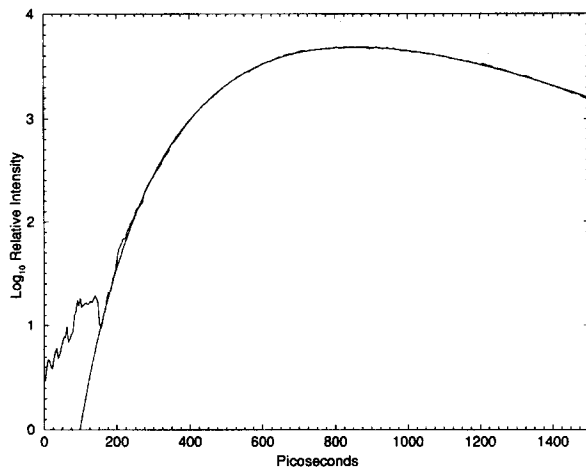


FIG. 5. The temporal distribution of transmitted light corresponding to the optical axis coinciding with the mask edge, plotted on a log scale, and a least-squares fit of the PCW model of photon transport.

geneous. The presence of the mask would be expected to limit the accuracy with which a model for a homogeneous medium can represent the temporal data. In order that the models could represent as accurately as possible the shape of the temporal data over the shorter photon flight times, models were fitted only over the first nanosecond. Despite the mask, we observed that both models were able to adequately represent the entire shape of the majority of the temporal profiles, and represent the first nanosecond of all the profiles, even when the mask was furthest across the optical axis. To decrease sensitivity to noise it was desirable to fit over the longest possible period, and 1 ns was found to be the approximate maximum period over which both models were able to achieve a good fit to all profiles. A second reason to restrict the fit to the first 1000 ps was because the nonlinear distortion of the temporal axis is worst nearest either end of the temporal profile. An example of the apparent ability of these models for photon transport to represent the data is illustrated in Fig. 5. This shows the temporal distribution obtained when the optical axis exactly coincided with the mask edge, and the PCW model prediction obtained using a least-squares fitting algorithm. Both are plotted on a log scale. Despite the gross inhomogeneity within the object, the shape is still well represented, albeit with fit parameters (i.e., optical coefficients) which may not be meaningful. Residual low intensity noise causes a departure between the model and data for times less than 170 ps. Similar fits were obtained over the first nanosecond of all 51 data profiles. A second set of ERFs were then obtained by integrating the model profiles for Δt in the range from 20 to 1000 ps. The results presented hereafter represent those obtained using the PCW model. However, the results obtained using the GWN model are almost identical.

Figure 6 shows the ERF obtained from an integration of the model fits to the temporal profiles at an integration time of $\Delta t = 100$ ps. Unlike the ERF generated from the data itself, shown in Fig. 3, this clearly identifies the edge of the mask. Also shown in Fig. 6 is a least-squares-fitted ERF

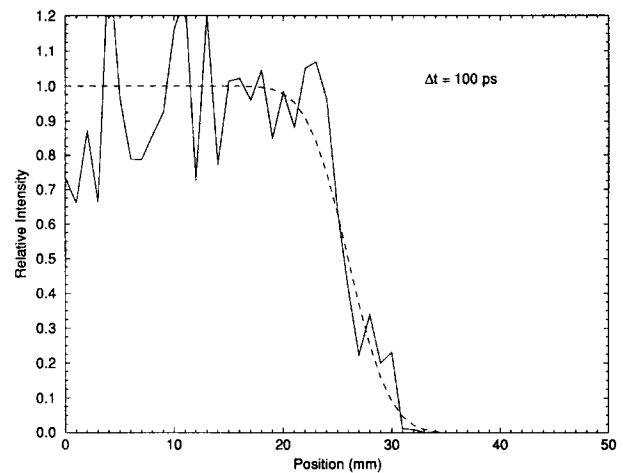


FIG. 6. The ERF obtained from an integration of the model fits to the temporal profiles at an integration time of $\Delta t = 100$ ps, and the corresponding least-squares fit of the ERF model.

model, which corresponds to a spatial resolution of 8.8 ± 3.1 mm. The fairly large uncertainty derived from the fitting process results from the observed "noise" in the ERF. We carefully considered possible sources of this noise, which becomes less significant as Δt increases. The photon transport model fits themselves are, of course, noiseless. Because the fits are made over the first nanosecond of data, the influence of residual background intensity is unlikely to be a source of such a large random fluctuation in the ERF profile. In fact, one significant and important advantage of using temporal extrapolation is that it is very insensitive to low power background noise on individual temporal distributions. We concluded that the random fluctuation is most likely due to imprecise calibration of the temporal axis. We consider two possible sources of error. First, a linear error due to the uncertainty involved in the location and centering of the reference pulses, which is performed in order to define the zero on each temporal axis. And second, the correction made for the nonlinearity in the temporal axis, discussed earlier, will be imprecise. The conclusion that these might be the cause was based on the observation that a very small temporal (i.e., horizontal) shift, say 5 ps, applied to a model profile produces a large percentage change in the integrated intensity at $\Delta t = 100$ ps, but very little percentage change at much larger values of Δt . This is because of the very rapid exponential-like rise of the curves over the first 200 ps or so. Since the temporal resolution of the system was estimated to be about 20 ps, an uncertainty of several picoseconds in the centering of the reference pulses is feasible. An alternative source of error may be due to the utilization of finite temporal sampling. Temporal distributions are sampled by effectively integrating light over 512 separate time windows. The flight time corresponding to each small window can be considered to be the center of the window. However, over a region where the gradient of the temporal distribution changes rapidly, the actual mean photon flight time will be somewhat different from the center time. Therefore a small random

distortion of the temporal profile occurs, on the scale of about half the sampling interval. However, for the data here where the temporal sampling is roughly every 4.5 ps, the error will occur on a scale of a couple of picoseconds, suggesting that other calibration errors will dominate.

An approximate correction for possible error in the linear adjustment was attempted as follows. First, we examined each model profile and calculated the time t_1 at which each model corresponds to a fixed intensity I_1 . If the temporal axis of each model profile were perfectly aligned and calibrated then it would be reasonable to expect that t_1 would vary smoothly as the optical axis was translated across the object. The assumption of smoothness is based on the fact that our sampling interval (1 mm) was well below the expected spatial resolution for an object embedded in the center of the scattering medium. If non-linearity errors are not significant, then any value of I_1 can be chosen which is common to all the model profiles. In practice we selected a value of I_1 corresponding to the approximate intensity at a time of 100 ps when the optical axis was furthest from the mask. If nonlinearity error is not negligible, this choice of I_1 would preferentially correct the error for an integration time of 100 ps, but the error would still exist, and may even increase, for integration times considerably larger or smaller. Since we are most interested in obtaining the highest resolution, corresponding to $\Delta t < 200$ ps, this choice of I_1 seems reasonable. The values of t_1 derived for this intensity, arranged as a function of displacement across the object, revealed an underlying smooth trend due to the presence of the mask, plus an expected random fluctuation of a few picoseconds. The smooth trend was removed by subtraction of a suitable polynomial fit to the distribution. The result represented our estimates of the additional shifts required in order to remove the linear error in the temporal alignment. These additional shifts, almost all within ± 5 ps, were applied to the model profiles and the ERFs at all integration times were recalculated. The new ERF obtained at an integration time of $\Delta t = 100$ ps is shown in Fig. 7. The edge response is considerably less noisy than that obtained previously, and the shift correction has not caused any noticeable loss in the edge sharpness. A least-squares-fitted ERF model, also shown, corresponds to a spatial resolution of 7.0 ± 0.6 mm. A similar improvement in ERF profiles was observed for all Δt less than 300 ps. For larger integration times the ERF profiles were slightly degraded, however, suggesting that the required shift is dependent upon position along the temporal axis, or in other words the nonlinearity error is not entirely negligible, at least over several hundred picoseconds.

Once again, spatial resolution was estimated for each ERF from a least-squares fit of Bentzen's ERF model. Figure 8 shows the values of spatial resolution Δx and their associated uncertainties plotted against Δt . The improvement in spatial resolution as Δt decreases is evident again, but now we observe sub-centimeter resolution at $\Delta t < 200$ ps. We observed that for Δt less than about 20 ps the ERFs become noisier without discernable further improvement in spatial resolution. Note that the uncertainty in the ERF model estimation at 100 ps is less because the ERF data are smoothest at $\Delta t = 100$ ps. This is due to having shifted the profiles

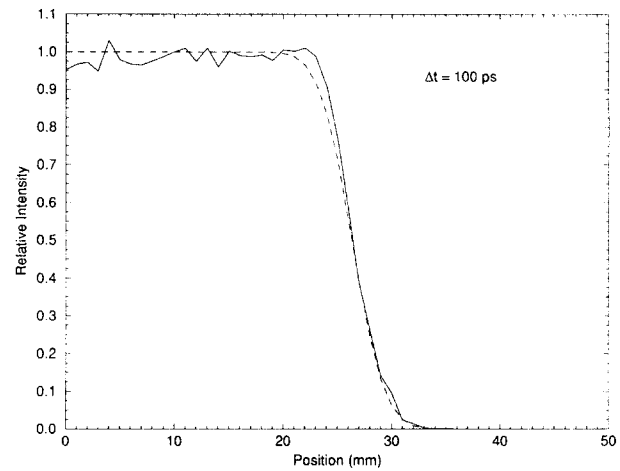


FIG. 7. The ERF obtained from an integration of the model fits to the temporal profiles at an integration time of $\Delta t = 100$ ps, following a linear adjustment of the temporal axis of each fit. Also shown is a least-squares fit of the ERF model.

slightly so that the variation in intensity is smooth at a time of 100 ps. Residual nonlinearity still produces noise in edge profiles at smaller and larger integration times, resulting in larger uncertainties. Uncertainty decreases again at very large Δt as sensitivity to a slight temporal shift decreases.

V. DISCUSSION

Although highly encouraging, the apparent effectiveness of this method of improving the spatial resolution performance of time-resolved imaging may be somewhat surprising. It is evident from the temporal profiles of the transmitted light, such as the one shown in Fig. 5, that there is almost no signal detected within the first 200 ps, and the model fitting process cannot have produced a meaningful "fit" at such short flight times. Therefore any high-resolution information must have been extracted from the data at longer flight times.

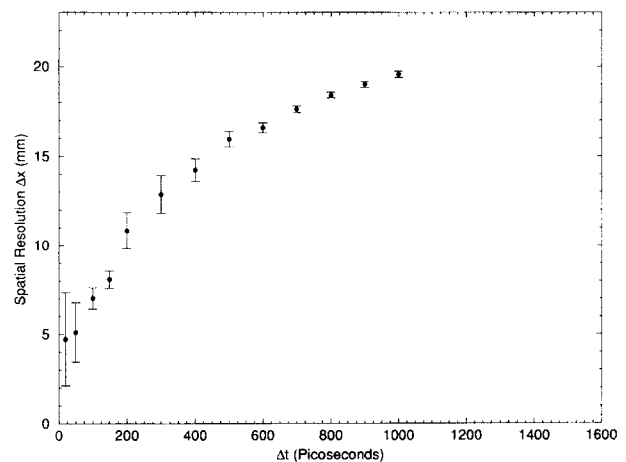


FIG. 8. The estimated spatial resolution as a function of integration time derived from the least-squares fits of the PCW model of photon transport.

It is not surprising that it should be possible to derive high-resolution information from the general shape of a temporal profile of transmitted light, but it is curious that it should be achievable using such relatively simple models of photon transport. Both of the models we investigated assume isotropic scatter through an infinite, homogenous slab, which was unrealistic on all counts. Furthermore, the diffusion approximation model involves an assumption that a nonzero photon density occurs everywhere at the instant a pulse is incident on the surface. Consequently it is not particularly appropriate for studying short flight-time photons.

As the optical axis was translated across the object containing the opaque mask, the distribution of detected light as a function of time changed, and there occurred a change in the corresponding fit parameters of the models. The models do not include a description of the inhomogeneity, and therefore the model fitting process essentially involves deriving the optical characteristics of an unbounded homogeneous slab, a "uniform slab equivalent," which would produce a temporal distribution (over the first nanosecond) as close as possible to that obtained through the object. It was evident that even when the mask overlapped the optical axis by as much as 25 mm, either model appeared able to closely represent the shape of the first nanosecond of the temporal data.

Throughout the experiment we were not concerned about the specific values of the optical coefficients that resulted from each fit. We noted, incidentally, that the optical coefficients did not tend to vary particularly smoothly as a function of displacement across the edge of the mask. An attempt, described elsewhere,²³ to generate images using the fit parameters themselves, revealed that, in order for the presence of small inhomogeneities to produce a smooth variation, the number of free parameters in the PCW model needed to be reduced from four to three. Here, however, we allowed the model to produce the best possible representation of the data profiles irrespective of how unrealistic the fit parameters might appear or how they might fluctuate during translation across the edge. In fact, for several temporal profiles obtained when the mask was furthest across the optical axis, the best fit of the PCW model was obtained with a negative absorption coefficient!

During the data analysis we were able to improve our estimate of some of the low- Δt edge responses by performing a first-order correction for uncertainty in the temporal calibration of the data, as described above. This was achieved via the application of *a priori* information. Specifically, we assumed that the intensity and temporal variation in the data profiles as the mask edge was translated across the optical axis should be smooth. However, in a general case where inhomogeneities might exist closer to either surface, where spatial resolution would be inherently superior and of the order of the sampling interval (1 mm), such an assumption would not necessarily be valid. Nevertheless, we anticipate that the application of *a priori* information may have a valuable role to play in the development of time resolved imaging as a diagnostic utility.

Methods of improving the spatial resolution of an imaging system by extrapolating its MTF, either directly or indirectly, to spatial frequencies beyond the inherent limit of the system

are generally known as "superresolution".²⁴ It would probably be inaccurate, however, to place the method presented here in this category. We think that it is more likely that the high spatial frequency information is already present in the measured temporal distribution of longer pathlength photons. It has been possible to extract that information by extrapolating the distributions to shorter pathlengths using a smooth mathematical model. It is feasible that the precise form of the model is irrelevant, and that an arbitrary polynomial with a large enough number of terms could have performed just as adequately. Conversely, perhaps alternative models able to describe the effects of anisotropic scatter and of inhomogeneities within a scattering medium would produce superior results. Both possibilities are currently the subjects of further study.

Although we have demonstrated that temporal extrapolation can be effective, we have yet to establish what factors limit the degree to which spatial resolution can be improved. One would expect, for example, the achievable spatial resolution to be limited, ultimately, by the finite temporal resolution of the system, since this limits the accuracy with which the temporal distributions can be measured. For the experiment described above, no improvement in the spatial resolution was observed for Δt decreased below about 20 ps. However, it is unlikely that the extrapolation method can always produce a gain in spatial resolution limited only by the temporal resolution. It is more likely that the achievable gain in spatial resolution will depend upon the period of time over which temporal profiles can be extrapolated with reasonable accuracy. Thus for a given system the resolution limit will still depend upon the minimum photon flight time at which a measurable flux of photons is obtained. For this experiment, the minimum was about 200 ps. In an endeavor to image through objects with properties matched as precisely as possible to the human breast, work is already in progress to test the method for media at which the transmitted flux is immeasurable for Δt as large as 300 or 400 ps.

ACKNOWLEDGMENTS

This research is supported by the Wellcome Trust, EPSRC, and Hamamatsu Photonics KK.

¹E. Silverberg, C. C. Boring, and T. S. Squires, "Cancer Statistics," *Ca-A Cancer J. Clinicians* **40**, 9-27 (1990).

²"Breast Cancer Screening Report," by a working group chaired by Prof. P. Forrester for the D.H.S.S. (H.M.S.O., UK, 1986).

³M. Cutler, "Transillumination as an aid in the diagnosis of breast lesions," *Surg. Gynecol. Obstet.* **48**, 721-728 (1929).

⁴B. Monsees, J. M. Destouet, and D. Gersell, "Light scan evaluation of nonpalpable breast lesions," *Radiology* **163**, 467-470 (1987).

⁵V. G. Peters, D. R. Wyman, M. S. Patterson, and G. L. Frank, "Optical properties of normal and diseased human breast tissues in the visible and near infrared," *Phys. Med. Biol.* **35**, 1317-1334 (1990).

⁶B. Chance and R. R. Alfano (Eds.), *Photon Migration and Imaging in Random Media and Tissues*, Proc. Soc. Photo-Opt. Instrum. Eng. **1888** (1993).

⁷G. Müller (Ed.), *Medical Optical Tomography: Functional Imaging and Monitoring*, SPIE Inst. Advan. Opt. Technol. **IS11** (1993).

⁸E. Leith, C. Chen, H. Chen, Y. Chen, D. Dilworth, J. Lopez, J. Rudd, P.-C. Sun, J. Valdmans, and G. Vossler, "Imaging through scattering media with holography," *J. Opt. Soc. Am. A* **9**, 1148-1153 (1992).

- ⁹L. Wang, P. P. Ho, C. Liu, G. Zhang, and R. R. Alfano, "Ballistic 2D imaging through scattering walls using an ultrafast optical Kerr gate." *Science* **253**, 769–771 (1991).
- ¹⁰M. D. Duncan, R. Mahon, L. L. Tankersley, and J. Reintjes, "Time-gated imaging through scattering media using stimulated Raman amplification." *Opt. Lett.* **16**, 1868–1870 (1991).
- ¹¹K. M. Yoo, B. B. Das, and R. R. Alfano, "Imaging of a translucent object hidden in a highly scattering medium from the early portion of the diffuse component of a transmitted ultrafast laser pulse." *Opt. Lett.* **17**, 958–960 (1992).
- ¹²J. C. Hebden, R. A. Kruger, and K. S. Wong, "Time resolved imaging through a highly scattering medium," *Appl. Opt.* **30**, 788–794 (1991).
- ¹³S. Andersson-Engels, R. Berg, S. Svanberg, and O. Jarlman, "Time resolved transillumination for medical diagnostics." *Opt. Lett.* **15**, 1179–1181 (1990).
- ¹⁴J. C. Hebden, "Evaluating the spatial resolution of a time resolved optical imaging system," *Med. Phys.* **19**, 1081–1087 (1992).
- ¹⁵A. H. Gandjbakhche, R. Nossal, and R. F. Bonner, "Resolution limits for optical transillumination of abnormalities deeply embedded in tissues." *Med. Phys.* **21**, 185–191 (1994).
- ¹⁶J. A. Moon, R. Mahon, M. D. Duncan, and J. Reintjes, "Resolution limits for imaging through turbid media with diffuse light," *Opt. Lett.* **18**, 1591–1593 (1993).
- ¹⁷J. C. Hebden, "Time resolved attenuation of transmitted laser pulses by a homogeneous scattering medium," *Opt. Lett.* **17**, 444–446 (1992).
- ¹⁸G. Zaccanti and P. Donelli, "Attenuation of energy in time-gated transillumination imaging: numerical results," *Appl. Opt.* **33**, 7023–7030 (1994).
- ¹⁹J. C. Hebden and D. T. Delpy, "Enhanced time-resolved imaging with a diffusion model of photon transport," *Opt. Lett.* **19**, 311–313 (1994).
- ²⁰M. S. Patterson, B. Chance, and B. C. Wilson, "Time resolved reflectance and transmittance for the non-invasive measurement of tissue optical properties," *Appl. Opt.* **28**, 2331–2336 (1989).
- ²¹A. H. Gandjbakhche, G. H. Weiss, R. F. Bonner, and R. Nossal, "Photon pathlength distributions for transmission through optically turbid slabs," *Phys. Rev. E* **48**, 810–818 (1993).
- ²²S. M. Bentzen, "Evaluation of the spatial resolution of a CT scanner by direct analysis of the edge response function," *Med. Phys.* **10**, 579–581 (1983).
- ²³J. C. Hebden, "Imaging through scattering media using characteristics of the temporal distribution of transmitted laser pulses," *Opt. Lasers Technol.* **26** (in press).
- ²⁴S. H. Lee, *Optical Information Processing* (Springer-Verlag, New York, 1981).